

TDHF and a macroscopic aspect of low-energy nuclear reactions

Kouhei Washiyama^{1,*}, Kazuyuki Sekizawa^{2,3}

¹Research Center for Superheavy elements, Kyushu University, Fukuoka, Japan

²Center for Transdisciplinary Research, Institute for Research Promotion, Niigata University, Niigata, Japan

³Division of Nuclear Physics, Center for Computational Sciences, University of Tsukuba, Ibaraki, Japan

Correspondence*:

Kouhei Washiyama

washiyama@phys.kyushu-u.ac.jp

ABSTRACT

Time-dependent Hartree–Fock (TDHF) method has been applied to various low-energy nuclear reactions, such as fusion, fission, and multinucleon transfer reactions. In this Mini Review, we summarize recent attempts to bridge a microscopic nuclear reaction theory, TDHF, and a macroscopic aspect of nuclear reactions through nucleus–nucleus potentials and energy dissipation from macroscopic degrees of freedom to microscopic ones obtained from TDHF in various colliding systems from light to heavy mass regions.

Keywords: Heavy-ion fusion reactions, TDHF, nucleus–nucleus potential, energy dissipation, fusion hindrance, quasifission

1 INTRODUCTION

Time-dependent Hartree–Fock (TDHF) method has been widely used in analyzing low-energy nuclear reactions since Bonche and his coworkers applied TDHF to collision of slabs in one-dimensional space as the first application of TDHF to nuclear physics [1]. Since then TDHF has been improved in several respects, e.g., including all terms in recent energy density functionals (EDF) such as Skyrme [2] and Gogny [3] functionals and breaking symmetries such as space (from one-dimensional to three-dimensional space).

It is well known that the coupling between relative motions of colliding nuclei (macroscopic degrees of freedom) and internal excitations of them (microscopic degrees of freedom) plays an important role for describing low-energy nuclear reactions at energies around the Coulomb barrier. To include such couplings, coupled-channel models [4, 5, 6, 7] have been developed and widely used. TDHF automatically includes couplings between relative motion and internal excitations since TDHF describes the dynamics of single particles. Moreover, TDHF provides an intuitive picture of nuclear dynamics through the time evolution of one-body densities constructed from single-particle wave functions in nuclei. Recently, TDHF has been applied to nuclear collective excitations [8, 9, 10, 11, 12, 13, 14, 3, 15] and to nuclear reactions such as fusion [16, 17, 18, 19, 20, 21, 22], quasifission [23, 24, 25], fission [26, 27, 28, 29], and multinucleon transfer reactions [30, 31, 32, 33, 34], some of which include pairing correlations.

In this Mini Review, however, we do not discuss the development of TDHF itself (see recent review articles on the development of TDHF in Refs. [35, 36, 37, 38, 39, 40]). Instead, we focus on a macroscopic aspect of low-energy nuclear reactions described by TDHF. To this end, we show various applications of the method called “dissipative-dynamics TDHF” (DD-TDHF) developed in Refs. [19, 20, 41].

2 DISSIPATIVE-DYNAMICS TDHF

The basic idea of DD-TDHF is to combine microscopic dynamics of nuclear reactions described by TDHF and a macroscopic aspect of nuclear reactions through a mapping from microscopic TDHF evolution to a set of macroscopic equations of motion. We briefly summarize DD-TDHF by the following steps: (1) We first solve the TDHF equation to obtain time evolution of single-particle wave functions for nuclear reactions:

$$i\hbar\frac{\partial\phi_i(t)}{\partial t} = \hat{h}[\rho(t)]\phi_i(t), \quad (1)$$

where $\phi_i(t)$ is the single-particle wave functions with index i (including spin and isospin degrees of freedom), and $\hat{h}[\rho(t)]$ is the single-particle Hamiltonian as a functional of one-body density $\rho(t)$, obtained from an EDF $E[\rho]$ by an appropriate functional derivative $\hat{h}[\rho(t)] = \delta E/\delta\rho$. (2) The next step is to define macroscopic two-body dynamics from microscopic TDHF simulations. Macroscopic two-body dynamics can be constructed once collective coordinate is defined from TDHF simulations. To do so in TDHF, we introduce a separation plane which divides the density $\rho(\mathbf{r}, t)$ of a colliding system to two subsystems, $\rho_1(\mathbf{r}, t)$ and $\rho_2(\mathbf{r}, t)$, corresponding to projectile-like and target-like densities. This separation plane is perpendicular to the collision axis, and at the position where the two densities $\rho_P(\mathbf{r}, t)$ and $\rho_T(\mathbf{r}, t)$ constructed from the single-particle wave functions initially in the projectile and in the target, respectively, cross. (See Fig. 1 of Ref. [19] for an illustrative example.) We then compute the coordinate R_i and its conjugated momentum P_i for each subsystem $i = 1, 2$ from $\rho_1(\mathbf{r}, t)$ and $\rho_2(\mathbf{r}, t)$. Also, we compute the masses of the two subsystems by $m_i = P_i/\dot{R}_i$. From these, two-body dynamics for the relative distance R as a collective coordinate and its conjugated momentum P , and reduced mass μ that may depend on R is constructed. (3) For the case of central collisions, we assume that the trajectory of the two-body dynamics obtained from TDHF follows a one-dimensional equation of motion for relative motions,

$$\frac{dR}{dt} = \frac{P}{\mu}, \quad (2)$$

$$\frac{dP}{dt} = -\frac{dV}{dR} - \frac{d}{dR}\left(\frac{P^2}{2\mu}\right) - \gamma\frac{P}{\mu}, \quad (3)$$

where $V(R)$ and $\gamma(R)$ denote the nucleus–nucleus potential and friction coefficient expressing energy dissipation from the relative motion of colliding nuclei to internal excitations in nuclei, respectively. An important point is that these two quantities $V(R)$ and $\gamma(R)$ are unknown in TDHF simulations. (4) To obtain those two unknown quantities we prepare a system of two equations from two trajectories at slightly different energies. Then, we solve the system of two equations at each R to obtain $V(R)$ and $\gamma(R)$. The details of numerical procedures for the calculations described above can be found in Refs. [19, 20, 41]. In the following results, we used the SLy4d Skyrme EDF [16] without pairing interactions.

3 NUCLEUS–NUCLEUS POTENTIAL AND ENERGY DISSIPATION

3.1 Light and medium-mass systems

In light and medium-mass systems, whose charge product $Z_1 Z_2$ is smaller than ≈ 1600 , it is known that fusion occurs once two nuclei contact each other after passing the Coulomb barrier. Indeed, TDHF simulations for head-on collisions at energies above the Coulomb barrier lead to fusion, keeping a compound system compact for sufficiently long time. We first provide selected results of nucleus–nucleus potential and energy dissipation obtained from DD-TDHF and discuss their properties.

In Fig. 1A, we show obtained nucleus–nucleus potentials as a function of relative distance R near the Coulomb barrier radius for $^{40}\text{Ca} + ^{40}\text{Ca}$. The lines show the nucleus–nucleus potentials at different center-of-mass energies ($E_{\text{c.m.}}$) by DD-TDHF, while the filled circles show the potential obtained by the frozen-density approximation, where the energy of the system is calculated with the same EDF except that the dynamical effect during the collision is neglected and the density of each fragment is fixed to be its ground-state one. Moreover, in the frozen-density approximation, the Pauli principle is neglected between nucleons in the projectile and in the target, leading to worse approximation as the overlap of projectile and target nuclei becomes significant. Important remarks from this figure are: (1) Potentials obtained at higher energies ($E_{\text{c.m.}} = 90, 100 \text{ MeV}$) agree with the frozen-density one, indicating the convergence of the potentials obtained by DD-TDHF at higher energies. (2) DD-TDHF potentials express an $E_{\text{c.m.}}$ dependence at lower energies $E_{\text{c.m.}} = 55, 57 \text{ MeV}$. (3) The height of DD-TDHF potential decreases with decreasing $E_{\text{c.m.}}$. The Coulomb barrier height decreases from $\approx 54.5 \text{ MeV}$ at $E_{\text{c.m.}} = 90, 100 \text{ MeV}$ of DD-TDHF and of the frozen-density approximation to $\approx 53.4 \text{ MeV}$ at $E_{\text{c.m.}} = 55 \text{ MeV}$ of DD-TDHF. The above remarks can be understood by the dynamical reorganization of the TDHF density profile of each TDHF trajectory. Figure 1B shows the TDHF density $\rho(x, y, z = 0, t)$ at each R for $E_{\text{c.m.}} = 55$ (top panels) and 90 MeV (bottom panels). At $E_{\text{c.m.}} = 90 \text{ MeV}$, the shape of each ^{40}Ca density keeps its shape spherical, while at $E_{\text{c.m.}} = 55 \text{ MeV}$ the shape of each ^{40}Ca density deviates from its ground-state spherical shape as R becomes smaller. This is a dynamical reorganization of density during fusion reactions. This dynamical reorganization changes the shape of each nucleus when two nuclei approach sufficiently, then reduces the height of the nucleus–nucleus potential obtained by DD-TDHF. This dynamical reduction of the nucleus–nucleus potential is seen in various light- and medium-mass systems in Ref. [19].

We would like to note that, in the density-constrained TDHF (DC-TDHF) method [17], in which constrained Hartree–Fock calculation is performed to obtain the nucleus–nucleus potential under the condition that the density is constrained to the density obtained from TDHF at each time, similar $E_{\text{c.m.}}$ dependence of nucleus–nucleus potentials is seen in various colliding systems reported, e.g., in Refs. [18, 42, 43, 44]. Moreover, in the $^{40}\text{Ca} + ^{40}\text{Ca}$ system, we find no significant difference in the potential extracted by DD-TDHF and the one by DC-TDHF [44].

3.2 Heavy systems

Contrary to light and medium-mass systems described in Sec. 3.1, it was experimentally observed that fusion probability at energies near the Coulomb barrier is strongly hindered in heavy systems ($Z_1 Z_2 \geq 1600$) [45, 46]. The main origin of this hindrance has been considered as the presence of the quasifission process, where a composite system of two colliding nuclei reseparates before forming an equilibrated compound nucleus. This fusion hindrance indeed has been observed in TDHF e.g., in Refs. [35, 41, 47, 48]. Namely, TDHF simulations for head-on collisions at energies above the Coulomb barrier lead to touching configuration of a composite system, and then to reseparation after a while (several

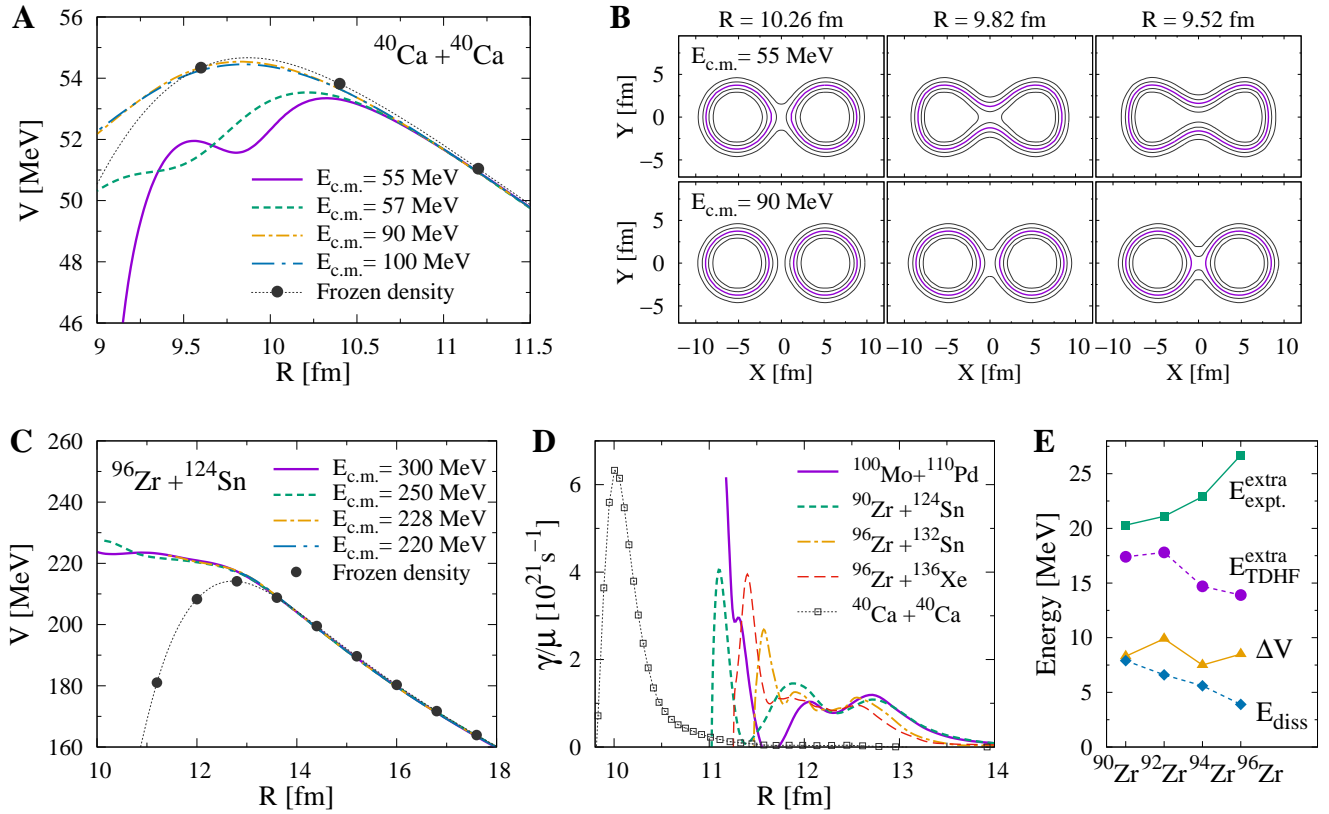


Figure 1. (A) Nucleus–nucleus potentials denoted by lines obtained by DD-TDHF at different energies and by the frozen-density approximation by filled circles with the dotted line as a function of R in $^{40}\text{Ca} + ^{40}\text{Ca}$. (B) Contour plots of density profile $\rho(X, Y, 0)$ obtained from TDHF at $E_{\text{c.m.}} = 55$ MeV (upper panels) and at $E_{\text{c.m.}} = 90$ MeV (lower panels), at $R = 10.26$ fm (left panels), 9.82 fm (middle), and 9.52 fm (right) in $^{40}\text{Ca} + ^{40}\text{Ca}$. The isodensities (contour lines) are plotted at each 0.025 fm^{-3} . (C) Same as (A) but for $^{96}\text{Zr} + ^{124}\text{Sn}$. (D) Friction coefficient divided by reduced mass, γ/μ , from DD-TDHF. (E) Extra-push energy from experiments ($E_{\text{expt.}}^{\text{extra}}$) and from TDHF ($E_{\text{TDHF}}^{\text{extra}}$) together with potential increase ΔV and dissipated energy E_{diss} for $^{90,92,94,96}\text{Zr} + ^{124}\text{Sn}$ (see text for detail). (A) and (B) adopted from [19], (C) and (D) adopted from [41], and (E) adopted from [41] with slight change with permission from APS and SciPris.

to tens of zeptoseconds). In Ref. [41], the extra-push energy $E_{\text{extra}}^{\text{TDHF}} = E_{\text{thres}}^{\text{TDHF}} - V_B^{\text{FD}}$ in TDHF was systematically obtained in heavy systems, where $E_{\text{thres}}^{\text{TDHF}}$ and V_B^{FD} denote the fusion threshold energy above which fusion occurs in TDHF and the Coulomb barrier energy obtained in the frozen-density approximation, respectively. We show in Fig. 1E extra-push energies in TDHF for $^{90,92,94,96}\text{Zr} + ^{124}\text{Sn}$, compared with those deduced from experimental data, $E_{\text{expt.}}^{\text{extra}}$, taken from [49], where the Bass barrier V_{Bass} [50] was employed as the Coulomb barrier height. We found that the difference between V_B^{FD} and V_{Bass} in $^{90,92,94,96}\text{Zr} + ^{124}\text{Sn}$ is at most ≈ 1 MeV. These obtained extra-push energies in TDHF reasonably reproduce observations.

One may think why the fusion hindrance in heavy systems appears in both experiments and TDHF simulations. In Ref. [41], we address this question and analyze where finite extra-push energies arise. For the analysis, we first derive the nucleus–nucleus potential and energy dissipation by DD-TDHF because we think that these two quantities are strongly related to the appearance of finite extra-push energy. In Fig. 1C, we show an example of nucleus–nucleus potentials extracted in heavy systems, which is for

the $^{96}\text{Zr} + ^{124}\text{Sn}$ system for three different energies in DD-TDHF and the frozen-density one. One can clearly see the difference between the potentials in $^{40}\text{Ca} + ^{40}\text{Ca}$ (Fig. 1A) and $^{96}\text{Zr} + ^{124}\text{Sn}$ (Fig. 1C): the potentials in $^{96}\text{Zr} + ^{124}\text{Sn}$ extracted by DD-TDHF monotonically increases as the relative distance decreases while the potentials in $^{40}\text{Ca} + ^{40}\text{Ca}$ and by the frozen-density approximation in $^{96}\text{Zr} + ^{124}\text{Sn}$ show a barrier structure at a certain relative distance. We have observed monotonic increase in potential in other heavy systems [41]. We consider the increase in potential in heavy systems as the transition from two-body dynamics of colliding nuclei to one-body dynamics of a composite system with strong overlap of the densities of colliding nuclei in TDHF and as the appearance of the conditional saddle point inside the Coulomb barrier in heavy systems [51, 52, 53, 54].

We would like to note here that this is different property from the one obtained from the DC-TDHF method in the same colliding system in Ref. [43]. This difference comes from a different interpretation of the nucleus–nucleus potential between the two methods. In the DC-TDHF method energy minimization is carried out at a given density of a system obtained from TDHF to deduce a nucleus–nucleus potential that eliminates internal excitations in this system. In the DD-TDHF method the potential is deduced under the assumption that TDHF evolution is reduced to a one-dimensional equation of motion for relative motion. We consider that the DD-TDHF potential can include a part of the DC-TDHF internal excitation energy. We make a comment on the origin of the difference between the two potentials in the following: In heavy systems with larger Coulomb repulsion, larger overlap of projectile and target densities during a collision in TDHF is achieved at a short relative distance. In TDHF, diabatic level crossings can occur more in larger overlap region, leading to a part of internal excitations and to a transition from two-body to one-body picture of a system. This part of internal excitations is interpreted as potential energy in DD-TDHF, while this is treated as excitation energy in DC-TDHF. In the DC-TDHF method, the flattening of the potential at short distances inside the Coulomb barrier radius is seen in heavier systems leading to the synthesis of superheavy elements in Ref. [42].

In Fig. 1D, reduced friction coefficient (γ/μ), the friction coefficient divided by the reduced mass extracted from Eq. (2), are plotted for selected systems. The friction coefficient increases as R decreases, and shows oscillations in heavy systems. We consider that the fact that the friction coefficient becomes negative indicates breakdown of the assumption that the TDHF trajectory follows a macroscopic one-dimensional equation of motion for relative motion of a two-body colliding system.

Finally we consider the origin of the fusion hindrance in heavy systems through the analysis with DD-TDHF. As mentioned above, nucleus–nucleus potential and energy dissipation are main contribution to the appearance of finite extra-push energy. We evaluate the potential increase at short distances and the accumulated dissipation energy from the friction coefficient using the formula [41],

$$E_{\text{diss}}(t) = \int_0^t dt' \gamma[R(t')] \dot{R}(t')^2, \quad (4)$$

up to time t when the kinetic energy of the relative motion of the system is completely dissipated. In Fig. 1E, we also show the contribution of potential increase ΔV and dissipated energy E_{diss} to the extra-push energy in the $^{90,92,94,96}\text{Zr} + ^{124}\text{Sn}$ systems. The result $\Delta V > E_{\text{diss}}$ indicates that the potential increase is a main origin for the appearance of the finite extra-push energy, i.e., fusion hindrance. Though the energy dissipation is known to play an important role in this fusion hindrance, it is not sufficient to explain the amount of the extra-push energy in the analysis with the DD-TDHF method.

3.3 Off-central collisions

So far, the applications of the DD-TDHF method has been limited to central collisions. Here we discuss a possible extension of the method to off-central collisions. Regarding (R, P) and (φ, L) as sets of canonical coordinates, where φ represents a rotation angle of the colliding system in the reaction plane and $L = \mu R^2 \dot{\varphi}$ is the angular momentum of the relative motion, we obtain a set of macroscopic equations of motion:

$$\frac{dR}{dt} = \frac{P}{\mu}, \quad (5)$$

$$\frac{d\varphi}{dt} = \frac{L}{\mu R^2}, \quad (6)$$

$$\frac{dP}{dt} = -\frac{dV}{dR} + \frac{1}{2} \left(\frac{P^2}{\mu^2} + \frac{L^2}{\mu^2 R^2} \right) \frac{d\mu}{dR} + \frac{L^2}{\mu R^3} - \gamma_R \frac{P}{\mu}, \quad (7)$$

$$\frac{dL}{dt} = -\gamma_\varphi \frac{L}{\mu}. \quad (8)$$

Here, $\gamma_R(R)$ and $\gamma_\varphi(R)$ denote the radial and tangential (or ‘‘sliding’’) friction coefficients, respectively, where the former already appeared in Eq. (3), the case of central collisions, and the latter governs the angular momentum dissipation [cf. Eq. (8)].

At first sight, there are three unknown quantities: the nucleus–nucleus potential V , the radial friction coefficient γ_R , and the tangential friction coefficient γ_φ . However, since time evolution of $\varphi(t)$ and $L(t)$ can be obtained from TDHF, a single TDHF simulation already provides the tangential friction coefficient by

$$\gamma_\varphi(R) = -\mu(t) \frac{\dot{L}(t)}{L(t)}. \quad (9)$$

Thus, there are only two unknown quantities in Eqs. (5)–(8), i.e. $V(R)$ and $\gamma_R(R)$, and we can apply the same procedure applied for central collisions.

In Fig. 2, we show the results for the $^{16}\text{O}+^{16}\text{O}$ reaction at $E/V_B = 1.4$ including off-central collisions, as an illustrative example. In Fig. 2A, the nucleus–nucleus potential is shown as a function of the relative distance, R . We also show the potential in the frozen-density approximation by open circles, for comparison. Figure 2A clearly shows that the method provides almost identical nucleus–nucleus potentials $V(R)$ irrespective of the impact parameters. In Fig. 2B, the effective potential $V_{\text{eff}}(R)$, the sum of nuclear, Coulomb, and centrifugal potentials, is shown. It can be seen that, for $b = 6$ fm, the closest distance is achieved at around $R = 10$ fm, at which the effective potential coincides with the incident relative energy. In Figs. 2C and 2D, the reduced radial and tangential friction coefficients, $\beta_R = \gamma_R/\mu$ and $\beta_\varphi = \gamma_\varphi/\mu$, are shown as a function of the relative distance. We found no significant dependence of the friction coefficients on the impact parameters in this system. In this way, this approach enables us to access the angular momentum dissipation mechanism and a systematic calculation is in progress.

Note that non-central effects on nucleus–nucleus potentials and effective mass parameters in fusion reactions have been studied in TDHF and DC-TDHF in Ref. [21]. It is interesting to make detailed comparison between those and our DD-TDHF in a future work.

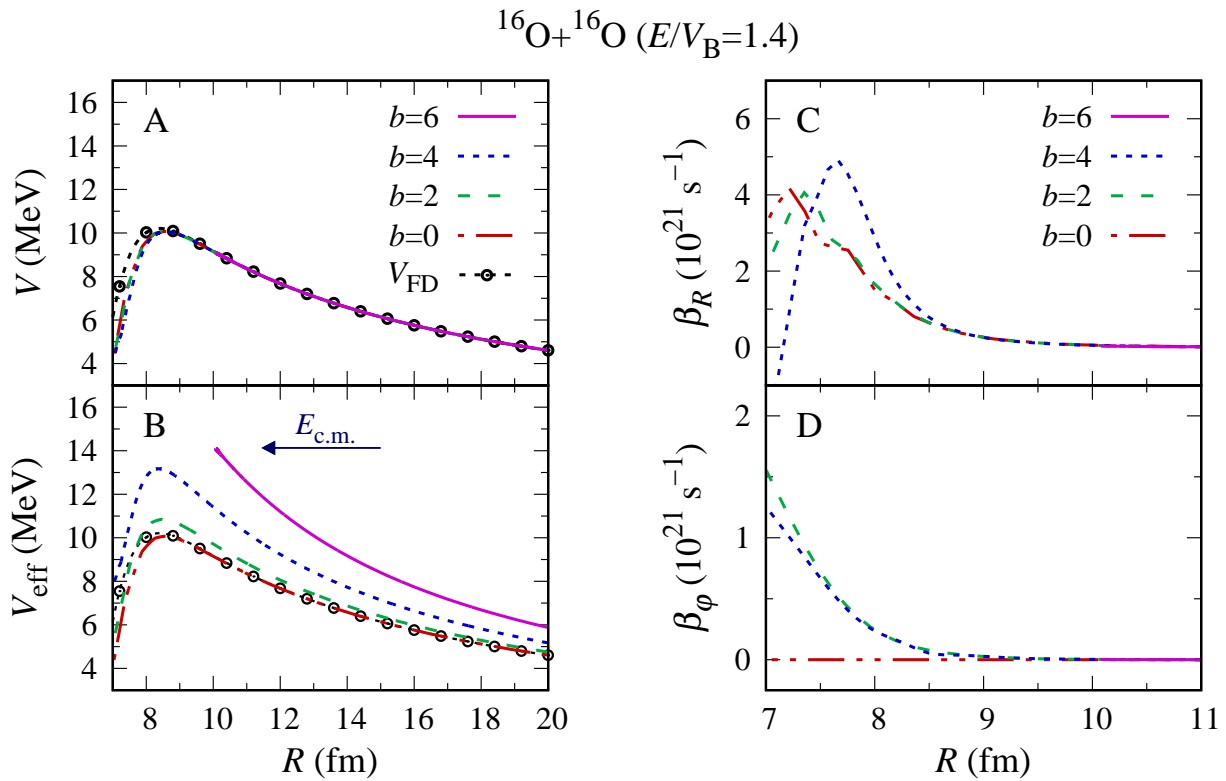


Figure 2. Results of DD-TDHF calculations for the $^{16}\text{O}+^{16}\text{O}$ reaction at $E/V_B = 1.4$ at various impact parameters. The nucleus–nucleus potentials and the effective potential $V_{\text{eff}}(R) = V(R) + L^2/2\mu R^2$ are shown in (A) and (B), respectively, as a function of the relative distance, R . The reduced radial friction coefficients, $\beta_R = \gamma_R/\mu$, are shown in (C), while the reduced tangential friction coefficients, $\beta_\phi = \gamma_\phi/\mu$, are shown in (D).

4 SUMMARY

The macroscopic aspect of TDHF dynamics for low-energy nuclear reactions at energies near the Coulomb barrier was discussed within the DD-TDHF method. We showed that the dynamical reorganization of single-particle wave functions inside the colliding nuclei affects the macroscopic nucleus–nucleus potential that leads to dynamical reduction of the potential around the Coulomb barrier radius in light- and medium-mass systems. In heavy systems, the dynamical reorganization leads to the fusion hindrance, increase in potential compared with the potential obtained from the frozen-density approximation in which the dynamical reorganization effect is neglected. By extending the DD-TDHF method to off-central collisions, the tangential friction coefficient was extracted in the $^{16}\text{O}+^{16}\text{O}$ reaction in addition to the nucleus–nucleus potential and the radial friction. As expected, the nucleus–nucleus potentials do not show a significant dependence of the initial angular momentum. The strength of the tangential friction is in the same order of magnitude as the radial one. From this extension, one can access the mechanism of angular momentum dissipation from microscopic reaction models. Possible future extension would be a systematic study of angular momentum dissipation mechanism in various systems, especially in heavy systems to address the fusion hindrance problem. Another possible extension would be a systematic study of collisions with deformed nuclei. It is interesting to study an orientation effect, a dependence of an angle between the collision axis and the principle axis of a deformed nucleus, on the nucleus–nucleus potential and the friction coefficient. It would be important to investigate how orbital angular momentum dissipation couples to a rotation of deformed nucleus during collision.

CONFLICT OF INTEREST STATEMENT

The authors declare that the research was conducted in the absence of any commercial or financial relationships that could be construed as a potential conflict of interest.

AUTHOR CONTRIBUTIONS

The manuscript was prepared by the authors.

FUNDING

The work was supported in part by QR Program of Kyushu University, by JSPS-NSFC Bilateral Program for Joint Research Project on Nuclear mass and life for unravelling mysteries of r-process, and by JSPS Grant-in-Aid for Early-Career Scientists No. 19K14704.

ACKNOWLEDGMENTS

The authors acknowledge Denis Lacroix and Sakir Ayik for the collaboration to this work. This work used computational resources of the Oakforest-PACS Supercomputer System provided by Multidisciplinary Cooperative Research Program in Center for Computational Sciences (CCS), University of Tsukuba (Project ID: NUCLHIC), and computational resources of the HPCI system (Oakforest-PACS) provided by Joint Center for Advanced High Performance Computing (JCAHPC) through the HPCI System Project (Project ID: hp190002).

REFERENCES

- [1] Bonche P, Koonin S, Negele JW. One-dimensional nuclear dynamics in the time-dependent hartree-fock approximation. *Phys. Rev. C* **13** (1976) 1226–1258. doi:10.1103/PhysRevC.13.1226.
- [2] Umar AS, Strayer MR, Reinhard PG. Resolution of the fusion window anomaly in heavy-ion collisions. *Phys. Rev. Lett.* **56** (1986) 2793–2796. doi:10.1103/PhysRevLett.56.2793.
- [3] Hashimoto Y. Linear responses in time-dependent hartree-fock-bogoliubov method with gogny interaction. *Eur. Phys. J. A* **48** (2012) 55. doi:10.1140/epja/i2012-12055-0.
- [4] Reisdorf W, Hessberger FP, Hildenbrand KD, Hofmann S, Münzenberg G, Schmidt KH, et al. Influence of collective surface motion on the threshold behavior of nuclear fusion. *Phys. Rev. Lett.* **49** (1982) 1811–1815. doi:10.1103/PhysRevLett.49.1811.
- [5] Dasso C, Landowne S, Winther A. Channel-coupling effects in heavy-ion fusion reactions. *Nucl. Phys. A* **405** (1983) 381 – 396. doi:https://doi.org/10.1016/0375-9474(83)90578-X.
- [6] Balantekin AB, Takigawa N. Quantum tunneling in nuclear fusion. *Rev. Mod. Phys.* **70** (1998) 77–100. doi:10.1103/RevModPhys.70.77.
- [7] Hagino K, Takigawa N. Subbarrier fusion reactions and many-particle quantum tunneling. *Prog. Theor. Phys.* **128** (2012) 1001–1060. doi:10.1143/PTP.128.1061.
- [8] Simenel C, Chomaz P, de France G. Quantum calculation of the dipole excitation in fusion reactions. *Phys. Rev. Lett.* **86** (2001) 2971–2974. doi:10.1103/PhysRevLett.86.2971.
- [9] Simenel C, Chomaz P. Nonlinear vibrations in nuclei. *Phys. Rev. C* **68** (2003) 024302. doi:10.1103/PhysRevC.68.024302.

- [10] Nakatsukasa T, Yabana K. Linear response theory in the continuum for deformed nuclei: Green's function vs time-dependent hartree-fock with the absorbing boundary condition. *Phys. Rev. C* **71** (2005) 024301. doi:10.1103/PhysRevC.71.024301.
- [11] Maruhn JA, Reinhard PG, Stevenson PD, Stone JR, Strayer MR. Dipole giant resonances in deformed heavy nuclei. *Phys. Rev. C* **71** (2005) 064328. doi:10.1103/PhysRevC.71.064328.
- [12] Avez B, Simenel C, Chomaz P. Pairing vibrations study with the time-dependent hartree-fock-bogoliubov theory. *Phys. Rev. C* **78** (2008) 044318. doi:10.1103/PhysRevC.78.044318.
- [13] Ebata S, Nakatsukasa T, Inakura T, Yoshida K, Hashimoto Y, Yabana K. Canonical-basis time-dependent hartree-fock-bogoliubov theory and linear-response calculations. *Phys. Rev. C* **82** (2010) 034306. doi:10.1103/PhysRevC.82.034306.
- [14] Stetcu I, Bulgac A, Magierski P, Roche KJ. Isovector giant dipole resonance from the 3d time-dependent density functional theory for superfluid nuclei. *Phys. Rev. C* **84** (2011) 051309. doi:10.1103/PhysRevC.84.051309.
- [15] Scamps G, Lacroix D. Systematics of isovector and isoscalar giant quadrupole resonances in normal and superfluid spherical nuclei. *Phys. Rev. C* **88** (2013) 044310. doi:10.1103/PhysRevC.88.044310.
- [16] Kim KH, Otsuka T, Bonche P. Three-dimensional tdhf calculations for reactions of unstable nuclei. *J. Phys. G* **23** (1997) 1267.
- [17] Umar AS, Oberacker VE. Heavy-ion interaction potential deduced from density-constrained time-dependent hartree-fock calculation. *Phys. Rev. C* **74** (2006) 021601. doi:10.1103/PhysRevC.74.021601.
- [18] Umar AS, Oberacker VE. Density-constrained time-dependent hartree-fock calculation of $^{16}\text{O} + ^{208}\text{Pb}$ fusion cross-sections. *Eur. Phys. J. A* **39** (2009) 243–247. doi:10.1140/epja/i2008-10712-5.
- [19] Washiyama K, Lacroix D. Energy dependence of the nucleus-nucleus potential close to the coulomb barrier. *Phys. Rev. C* **78** (2008) 024610. doi:10.1103/PhysRevC.78.024610.
- [20] Washiyama K, Lacroix D, Ayik S. One-body energy dissipation in fusion reactions from mean-field theory. *Phys. Rev. C* **79** (2009) 024609. doi:10.1103/PhysRevC.79.024609.
- [21] Jiang X, Maruhn JA, Yan S. Microscopic study of noncentral effects in heavy-ion fusion reactions with spherical nuclei. *Phys. Rev. C* **90** (2014) 064618. doi:10.1103/PhysRevC.90.064618.
- [22] Hashimoto Y, Scamps G. Gauge angle dependence in time-dependent hartree-fock-bogoliubov calculations of $^{20}\text{O} + ^{20}\text{O}$ head-on collisions with the gogny interaction. *Phys. Rev. C* **94** (2016) 014610. doi:10.1103/PhysRevC.94.014610.
- [23] Kedziora DJ, Simenel C. New inverse quasifission mechanism to produce neutron-rich transfermium nuclei. *Phys. Rev. C* **81** (2010) 044613. doi:10.1103/PhysRevC.81.044613.
- [24] Wakhle A, Simenel C, Hinde DJ, Dasgupta M, Evers M, Luong DH, et al. Interplay between quantum shells and orientation in quasifission. *Phys. Rev. Lett.* **113** (2014) 182502. doi:10.1103/PhysRevLett.113.182502.
- [25] Sekizawa K, Yabana K. Time-dependent hartree-fock calculations for multinucleon transfer and quasifission processes in the $^{64}\text{Ni} + ^{238}\text{U}$ reaction. *Phys. Rev. C* **93** (2016) 054616. doi:10.1103/PhysRevC.93.054616.
- [26] Simenel C, Umar AS. Formation and dynamics of fission fragments. *Phys. Rev. C* **89** (2014) 031601. doi:10.1103/PhysRevC.89.031601.
- [27] Scamps G, Simenel C, Lacroix D. Superfluid dynamics of ^{258}Fm fission. *Phys. Rev. C* **92** (2015) 011602(R). doi:10.1103/PhysRevC.92.011602.

- [28] Goddard P, Stevenson P, Rios A. Fission dynamics within time-dependent hartree-fock: Deformation-induced fission. *Phys. Rev. C* **92** (2015) 054610. doi:10.1103/PhysRevC.92.054610.
- [29] Bulgac A, Magierski P, Roche KJ, Stetcu I. Induced fission of ^{240}Pu within a real-time microscopic framework. *Phys. Rev. Lett.* **116** (2016) 122504. doi:10.1103/PhysRevLett.116.122504.
- [30] Simenel C. Particle transfer reactions with the time-dependent hartree-fock theory using a particle number projection technique. *Phys. Rev. Lett.* **105** (2010) 192701. doi:10.1103/PhysRevLett.105.192701.
- [31] Sekizawa K, Yabana K. Time-dependent hartree-fock calculations for multinucleon transfer processes in $^{40,48}\text{Ca} + ^{124}\text{Sn}$, $^{40}\text{Ca} + ^{208}\text{Pb}$, and $^{58}\text{Ni} + ^{208}\text{Pb}$ reactions. *Phys. Rev. C* **88** (2013) 014614. doi:10.1103/PhysRevC.88.014614.
- [32] Scamps G, Lacroix D. Effect of pairing on one- and two-nucleon transfer below the coulomb barrier: A time-dependent microscopic description. *Phys. Rev. C* **87** (2013) 014605. doi:10.1103/PhysRevC.87.014605.
- [33] Wu Z, Guo L. Microscopic studies of production cross sections in multinucleon transfer reaction $^{58}\text{Ni} + ^{124}\text{Sn}$. *Phys. Rev. C* **100** (2019) 014612. doi:10.1103/PhysRevC.100.014612.
- [34] Jiang X, Wang N. Probing the production mechanism of neutron-rich nuclei in multinucleon transfer reactions. *Phys. Rev. C* **101** (2020) 014604. doi:10.1103/PhysRevC.101.014604.
- [35] Simenel C. Nuclear quantum many-body dynamics. *Eur. Phys. J. A* **48** (2012) 152. doi:10.1140/epja/i2012-12152-0.
- [36] Nakatsukasa T. Density functional approaches to collective phenomena in nuclei: Time-dependent density functional theory for perturbative and non-perturbative nuclear dynamics. *Prog. Theor. Exp. Phys.* **2012** (2012) 01A207. doi:10.1093/ptep/pts016.
- [37] Nakatsukasa T, Matsuyanagi K, Matsuo M, Yabana K. Time-dependent density-functional description of nuclear dynamics. *Rev. Mod. Phys.* **88** (2016) 045004. doi:10.1103/RevModPhys.88.045004.
- [38] Simenel C, Umar A. Heavy-ion collisions and fission dynamics with the time-dependent hartree-fock theory and its extensions. *Prog. Part. Nucl. Phys.* **103** (2018) 19 – 66. doi:https://doi.org/10.1016/j.pnpnp.2018.07.002.
- [39] Sekizawa K. TdHF theory and its extensions for the multinucleon transfer reaction: A mini review. *Frontiers in Physics* **7** (2019) 20. doi:10.3389/fphy.2019.00020.
- [40] Stevenson P, Barton M. Low-energy heavy-ion reactions and the skyrme effective interaction. *Prog. Part. Nucl. Phys.* **104** (2019) 142 – 164. doi:https://doi.org/10.1016/j.pnpnp.2018.09.002.
- [41] Washiyama K. Microscopic analysis of fusion hindrance in heavy nuclear systems. *Phys. Rev. C* **91** (2015) 064607. doi:10.1103/PhysRevC.91.064607.
- [42] Umar AS, Oberacker VE, Maruhn JA, Reinhard PG. Entrance channel dynamics of hot and cold fusion reactions leading to superheavy elements. *Phys. Rev. C* **81** (2010) 064607. doi:10.1103/PhysRevC.81.064607.
- [43] Oberacker VE, Umar AS, Maruhn JA, Reinhard PG. Microscopic study of the $^{132,124}\text{Sn} + ^{96}\text{Zr}$ reactions: Dynamic excitation energy, energy-dependent heavy-ion potential, and capture cross section. *Phys. Rev. C* **82** (2010) 034603. doi:10.1103/PhysRevC.82.034603.
- [44] Umar AS, Simenel C, Oberacker VE. Energy dependence of potential barriers and its effect on fusion cross sections. *Phys. Rev. C* **89** (2014) 034611. doi:10.1103/PhysRevC.89.034611.
- [45] Gäggeler H, Sikkeland T, Wirth G, Bröchle W, Bögl W, Franz G, et al. Probing sub-barrier fusion and extra-push by measuring fermium evaporation residues in different heavy ion reactions. *Z. Phys. A* **316** (1984) 291–307. doi:10.1007/BF01439902.

- [46] Sahm CC, Clerc HG, Schmidt KH, Reisdorf W, Armbruster P, Heberger FP, et al. Hindrance of fusion in central collisions of heavy, symmetric nuclear systems. *Z. Phys. A* **319** (1984) 113–118. doi:10.1007/BF01415623.
- [47] Simenel C, Avez B, Golabek C. Microscopic description of heavy ion collisions around the barrier (2009). ArXiv:0904.2653.
- [48] Guo L, Nakatsukasa T. Time-dependent hartree-fock studies of the dynamical fusion threshold. *EPJ Web Conf.* **38** (2012) 09003. doi:10.1051/epjconf/20123809003.
- [49] Schmidt KH, Morawek W. The conditions for the synthesis of heavy nuclei. *Rep. Prog. Phys.* **54** (1991) 949.
- [50] Bass R. Fusion of heavy nuclei in a classical model. *Nucl. Phys. A* **231** (1974) 45–63. doi:http://dx.doi.org/10.1016/0375-9474(74)90292-9.
- [51] Swiatecki WJ. The dynamics of nuclear coalescence or reseparation. *Phys. Scr.* **24** (1981) 113–122.
- [52] Swiatecki WJ. The dynamics of the fusion of two nuclei. *Nucl. Phys. A* **376** (1982) 275–291. doi:http://dx.doi.org/10.1016/0375-9474(82)90065-3.
- [53] Bjornholm S, Swiatecki WJ. Dynamical aspects of nucleus-nucleus collisions. *Nucl. Phys. A* **391** (1982) 471–504. doi:http://dx.doi.org/10.1016/0375-9474(82)90621-2.
- [54] Świątecki WJ, Siwek-Wilczyńska K, Wilczyński J. Fusion by diffusion. ii. synthesis of transfermium elements in cold fusion reactions. *Phys. Rev. C* **71** (2005) 014602. doi:10.1103/PhysRevC.71.014602.